

# Influence of crustal fracturing on the thermal springs and earthquake swarms distribution in the north-east part of the Baikal rift system (Russia)

## *Influenza della fratturazione della crosta sulle sorgenti termali e sulla distribuzione degli sciami di terremoti nella parte nord-est del sistema del rift del Baikal (Russia)*

Anna Vladimirovna Novopashina, Elena Alexandrovna Kuz'mina

**Riassunto:** Le faglie del sistema di rift del lago Baikal, sviluppatesi in un recente periodo di rifting, sono caratterizzate da attività idrotermale e sismica. Il livello di fratturazione influisce sulla localizzazione delle venute termali e sulla distribuzione degli sciami sismici, prevalenti nella parte nordorientale del rift del Baikal. Le caratteristiche specifiche dell'interposizione di outputs idrotermali e sismicità, dipendenti dall'eterogeneità della fratturazione e dalla saturazione d'acqua degli strati di litosfera, non sono state valutate in precedenza. I risultati dell'analisi statistica dei dati idrotermali, mostrano come la maggior parte delle sorgenti sia distribuita in aree con densità di faglie più elevata. Le venute termali multiple a temperatura inferiore sono associate a zone di massima densità di interspazio tra blocchi. L'analisi della sismicità condotta nel tempo ha mostrato che le migrazioni di attività sismica di debole e moderata intensità, si propagano

attraverso queste zone. Gli sciami avviano il fronte di deformazione che si propaga nella porzione quasiplastica del mantello superiore ad una velocità di decine di chilometri all'anno, facendo potenzialmente aumentare la pressione di poro del fluido acquoso nella crosta terrestre inferiore, facilitare il movimento verso l'alto del fluido lungo la sezione e causare il processo di stress e successivo rilassamento in zone ad alto grado di fratturazione. Gli sciami sismici si verificano principalmente in aree a media densità di fratturazione, associate a faglie profonde che delimitano blocchi consolidati della crosta terrestre. Le venute idrotermali a temperatura elevata e media e con composizione chimica assimilabile a circuiti profondi sono correlate con tali zone.

**Keywords:** *Baikal rift system, thermal springs, earthquake swarms, interblock space, water fluid, basalt fluid, stress transfer.*

**Parole chiave:** sistema del Rift di Baikal, sorgenti termali, sciami sismici, fluidi acquosi, fluidi basaltici, trasferimento di stress.

**Abstract:** *The Baikal rift system faults, having developed in the recent rift formation period, are characterized by hydrothermal and seismic activity. Especially in the northeastern part, the level of fracturing affects the localization of thermal outlets and the distribution of earthquake swarms. The specific features of the hydrothermal outputs and seismicity interposition, depending on the fracture heterogeneity and water saturation of the lithosphere layers, have not been previously evaluated. The results of the statistical analysis of the hydrothermal data, presented herein, show that most of the springs are distributed in areas of increased fault density. Multiple less hot hydrotherms are associated with zones of maximum density in the inter-block space. The spatio-temporal analysis of seismicity showed that migrations of weak and moderate seismic activity propagate from earthquake swarms through these zones. Swarms initiate the deformation front by propagating in the quasiplastic layer of the upper mantle at a speed of tens of kilometers per year, which can increase the aqueous fluid pore pressure in the lower earth's crust, facilitate the movement of the fluid upwards along the section, and cause a process of successive stress relaxation in zones of high fracturing and concentration of hydrothermal springs. Earthquake swarms occur in areas of about average fracture density, associated with deep faults framing consolidated blocks of the earth's crust. The hydrotherms with high or average temperature, and with probable deep source chemical composition components are related with such zones.*

Anna Vladimirovna NOVOPASHINA ✉  
Institute of the Earth's Crust, Siberian Branch of RAS  
Irkutsk - Russian Federation  
avn\_crust@mail.ru

Elena Alexandrovna KUZ'MINA  
Institute of the Earth's Crust, Siberian Branch of RAS  
Irkutsk - Russian Federation

Ricevuto/Received: 15 November 2018-Accettato/Accepted: 01 March 2019  
Pubblicato online/Published online: 16 May 2019  
This is an open access article under the CC BY-NC-ND license:  
<http://creativecommons.org/licenses/by-nc-nd/4.0/>

© Associazione Acque Sotterranee 2019

## Introduction

The evolution of the Baikal rift system is evident in its tectonic, seismic and hydrothermal activity. The prevailing tensile tectonic stresses control the opening of faults as conductive channels for water. As a result, the watering of the active strike and strike-slip fault zones is much higher than the intact porous layers and the consolidated blocks of the earth's crust (Plyusnin 2008; Pola et al. 2015).

Underground fluids, active faults, and the seismic process are interdependent. Recent geodynamic processes, accompanied by seismicity, have a significant impact on rock permeability and groundwater circulation (Wang 2000; Lysak 2002; Shabynin et al. 2002; Jónsson et al. 2002; He and Peltzer 2010; Hughes et al. 2011; Boldina and Kopylova 2017; Ingebritsen and Gleeson 2017; Tung and Masterlark 2018; Tung et al. 2018). The effect of seismic injection causes a pressure difference, inducing filtration of groundwater in different directions (Parotidis et al. 2003; Ingebritsen et al. 2015; Tung and Masterlark 2018). The high permeability of cracks provides free water exchange, and the heat flow in the active faults zones contributes to an increase in its velocity (Plyusnin 2008).

Permeability may change in response to changes in the elastic stresses in the Earth's crust, for instance by strong earthquakes, swarms of earthquakes, or artificial fluctuations (Ingebritsen et al. 2015; He and Peltzer 2010; Hughes et al. 2011). After strong events, their aftershocks, as well as swarms of earthquakes, changes in the gas (Yoshioka et al. 1970) and ion-salt (Shitov et al. 2016) groundwater compositions, as well as changes in groundwater level and temperature are ascertained.

It is considered that thermal springs of the Baikal rift zone are formed at shallow depths (3–5 km), but processes occurring in the earthquake hypocenters and in the lower parts of active faults should be considered as one of the main energy sources of their formation (Pinneker et al. 1984).

In the faulting process, water, in turn, also plays an important role in the development of the earth's crust tectonic structures, reducing the strength of rocks and the coefficient of interblock friction, being both a trigger of earthquakes (Becken et al. 2011; Deng et al. 2016; Saar and Manga 2003) and earthquake swarms (Parotidis et al. 2003; Heinicke et al. 2009), and contributing to the relaxation of tectonic stress in the zone of critical tectonic load and the weakening of the shocks force (Acosta et al. 2018; Psakhier et al. 2004; Tung and Masterlark 2016). The fracture zones weakening by hydrothermal changes can also occur at seismogenic depths (Heinicke et al. 2009). It has been established that even large faults can be reactivated by intense perturbations of fluid pressures (Passelègue et al. 2018). The presence of fluid in the faults is associated with poroelastic deformation, and can be considered as one of the main parameters that contributes to an increase in elastic stresses and fault interaction (Kariche et al. 2018). For most seismic events, the trigger mechanism is the geodynamic stress accumulation and the critical pressure of a pore fluid. Aftershocks of earthquakes correlate with the pore pressure field (Tung et al. 2018). At the same time,

aftershocks or subsequent seismic events are either delayed (Tung and Masterlark 2018), or the relaxation of elastic stresses in a flooded tectonically active environment occurs as multiple and weaker events (Artyushkov 1993; Psakhie et al. 2004). The gradual propagation of fluids in different directions, caused by elastic stresses changing from strong events and their main aftershocks (Parotidis et al. 2003; Marone et al. 1991), occurs to a zone of lowest filtration resistance - zone of increased earth's crust fracturing.

Fluid migration caused by the seismic pumping effect occurs both horizontally and vertically (Tung et al. 2018). The proposed transition of fluids from the lower crust and upper mantle to the weakened (fractional) zone is a cause that stimulates seismicity and determines variations of its amplitude and activity along a strike (Becken et al. 2011). Therefore, fractional zones are characterized by the migration of clusters of weak and moderate seismic events caused by strong events or swarms of earthquakes. Strong earthquakes and earthquake swarms are located on the edges of migration sequences, associated with the boundary between maximum and minimum elastic stresses areas and the boundaries between consolidated blocks and fractured interblock space (Novopashina and Sankov 2018).

Fast migrations (i.e., during the first few hours, days, or months after an earthquake) are due to the response of the earth's crust elastic upper layer, as well as to fluid pore pressure changes (Marone et al. 1991).

The process of slow migration lasts for decades and is due to the stress transfer through the more plastic and deep layers of the lithosphere (Chéry et al. 2001; Pollitz et al. 2003; Freed 2005; Bürgmann and Dresen 2008). Such migrations are observed in many parts of the planet (cf. Reasenber and Simpson 1992; Redekek and Sacks 2001; Lin and Stein 2004; Hamling et al. 2014; Steacy et al. 2014), including the Baikal rift system (BRS) (Sherman 2013; Levina and Ruzhich 2015; Novopashina and Sankov 2018).

Our attention was attracted by the fact that in the northeastern part of the BRS hydrothermal springs are spatially related with zones of high fracturing and seismic activity migration. In this article we investigated how these phenomena can be related. This article presents the results of a spatial comparison of the density parameter of active faults ( $n$ ) with the number of thermal springs and the number of earthquake swarms. An attempt was also made to identify and explain the spatial relationship of the block and layered structure of the Earth's crust with the spread of seismicity and the outputs of modern hydrotherms.

## Data and Methods

The density of active faults (parameter  $n$ ) is defined as the number of faults per unit area. In order to avoid fractional values, the number of faults in the grid cell per unit area has not been divided by the cell area.

For the BRS territory,  $n$  is calculated on the basis of a digital map of active faults (Lunina 2016) (Fig. 1a) in a  $1^\circ \times 1^\circ$  cell with a  $0.5^\circ$  overlapping.

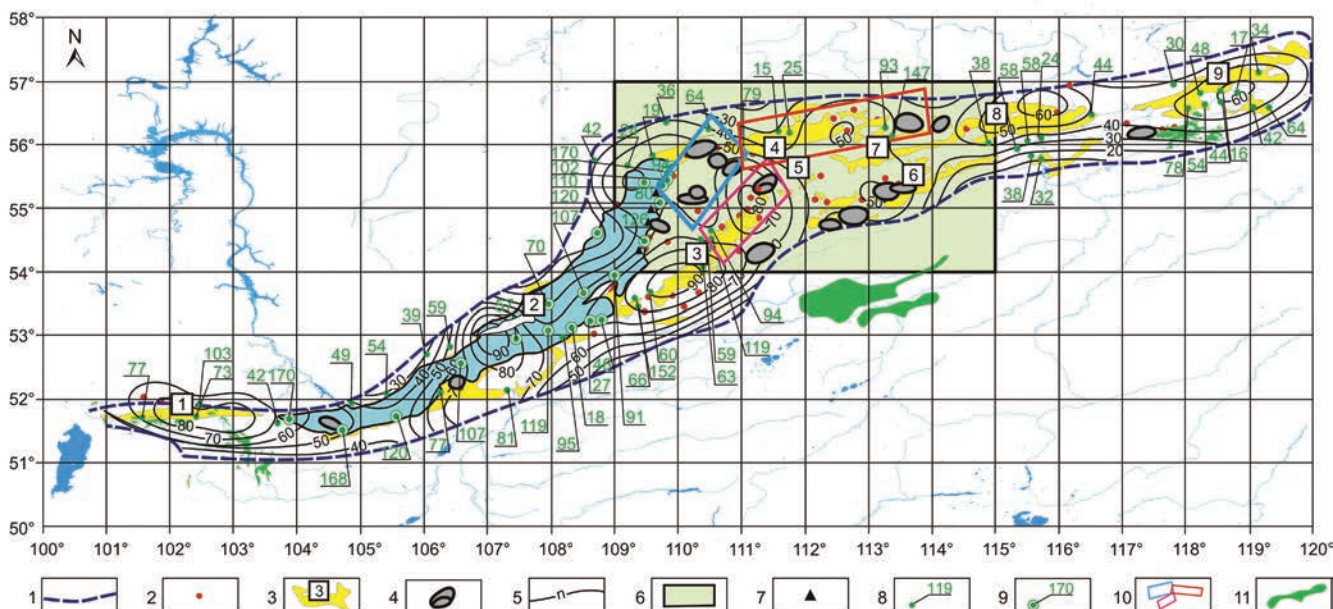


Fig. 1 - The Baikal rift system (Russia) map of active faults, thermal springs and earthquake swarms for the  $1^\circ \times 1^\circ$  cell size. 1 – BRS contour; 2 – thermal springs according to Tkachuk (1957); 3 – depressions with their numbers (in the squares: 1 – Tunkin, 2 – Baikal, 3 – Barguzin, 4 – Verkhneangara, 5 – Amut, 6 – Baunt, 7 – Muyakan, 8 – Muya, 9 – Chara); 4 – earthquake swarms, according to Solonenko and Solonenko (1987), Radziminovich et al. (2013), Melnikova et al. (2007); 5 – active faults density contour lines (n), according to Lunina (2016); 6 – research area contour of the BRS northeastern part detailed in Fig. 4; 7 – abnormally high heat flux points (from 297 to 37000  $\text{mW/m}^2$ ) (Golubev 2007); 8 – points of heat flux measurement with their values ( $\text{mW/m}^2$ ) inside the Baikal lake water area (Golubev 2007); 9 – points of heat flow measurement on land with their values ( $\text{mW/m}^2$ ) according to Golubev (2007), Lysak 2002; 10 – areas of seismic data projection; 11 – outcrops of volcanic rocks.

Fig. 1 - La carta del rift system del Baikal (Russia) relativa a faglie attive, sorgenti termali e sciami sismici per le celle di dimensioni  $1^\circ \times 1^\circ$ . 1 – BRS area; 2 – sorgenti termali in accordo con Tkachuk (1957); 3 – depressioni con relativa numerazione (nei quadrati: 1 – Tunkin, 2 – Baikal, 3 – Barguzin, 4 – Verkhneangara, 5 – Amut, 6 – Baunt, 7 – Muyakan, 8 – Muya, 9 – Chara); 4 – sciami di terremoti, in accordo con Solonenko and Solonenko (1987), Radziminovich et al. (2013) e Melnikova et al. (2007); 5 – linee di densità di faglie attive (n), in accordo con Lunina (2016); 6 – area della ricerca, parte nord est di BRS dettagli in figura 4; 7 – punti a flusso di calore anomalmente alto (da 297 a 37000  $\text{mW/m}^2$ ) (Golubev 2007); 8 – punti di misurazione del flusso di calore con i loro valori ( $\text{mW/m}^2$ ) all'interno dell'area del lago Baikal (Golubev 2007); 9 – punti di misurazione del flusso di calore sul terreno con i loro valori ( $\text{mW/m}^2$ ) in accordo con Golubev (2007) e Lysak (2002); 10 – aree di proiezione dei dati sismici; 11 – affioramenti di rocce vulcaniche.

In order to enlarge the scale for the northeastern part of the Baikal rift, characterized by multiple thermal outputs and earthquake swarms, the  $n$  parameter is also obtained in  $0.37^\circ \times 0.37^\circ$  cells, the size of which has been decided according to the mean thickness of the crust in this zone, i.e. 41 km or about  $0.37^\circ$  (Matz et al. 2001).

The density value refers to the cell center. For establishing the nature of the probability distribution of the fracture density value, the number of cells of each density is calculated and the modal, median and mean values of  $n$  are determined.

To determine the probability distribution character of the faults density for a  $0.37^\circ \times 0.37^\circ$  cell size, the number of cells of each density range has been calculated. The modal, median, and average values of the parameter  $n$  have been also determined.

Using grid size  $0.37^\circ \times 0.37^\circ$  for every density range, the total number of thermal springs (according to Tkachuk 1957) and the number of swarms in the cell (according to Solonenko and Solonenko 1987; Radziminovich et al. 2013; Melnikova et al. 2007) are obtained.

As an indicator of uncertainty of the hydrothermal springs and the swarms quantity (in cells) samples, the coefficient of variation has been determined by the formula:

$$V = \sigma / \bar{x}$$

where  $\sigma$  is the standard deviation,  $\bar{x}$  is the average value of the used parameter.

Besides the relative index of variation of the samples, the autocorrelation function of the first and second orders were calculated, that allow to estimate the randomness level of the result distributions:

$$r_L = \frac{\sum_{i=L+1}^n (x_{i-L} - \bar{x}_{i-L}) \cdot (x_i - \bar{x}_i)}{\sqrt{\sum_{i=L+1}^n (x_{i-L})^2 \cdot \sum_{i=L+1}^n (x_i - \bar{x}_i)^2}}$$

where  $r_L$  is the autocorrelation coefficient of the distribution value ( $x$ ), calculated for the shift of data  $L = 1, 2, \dots, n$ . Correlograms were calculated with an offset of 1 and 2 values.

The calculation of the autocorrelation function allows to determine whether neighboring values of the distribution function are statistically dependent on each other, or the process is due only to a random component. With a sharp decline in the correlogram function values to low values, the level of uncertainty will be high and the process can be considered conditioned only by a random component. A

gradual decrease of the correlogram values or the presence of significant correlation coefficient maximums in the correlogram function, mean a tendency in the analyzed parameter distribution and point out to parameter value allocation in a limited range.

The significance of the correlation was determined by using the test statistics of the correlation coefficient significance ( $t$ ), calculated by the formula:

$$t = \left( 0.5 \cdot \ln \frac{1+r}{1-r} - \frac{|r|}{2(n-1)} \right) \sqrt{n-3}$$

where  $n$  is the number of points in the sample, and  $r$  is the Pearson correlation coefficient.

To establish the presence of deep-seated components signs in the spring's thermal water, the chemical compositions of the Barguzin Depression hydrotherms were tested, including water sampling for macro- and microcomponents, gas composition and measurement of water temperature with a mercury thermometer. Using the physicochemical modeling program "Selector" (Kazmin 1979; Karpov 1981; Chudnenko 2003; Avchenko 2009) the measured chemical composition was compared with the model composition (as in Kuz'mina et al. 2015) obtained for models of the earth's crust and upper mantle, with and without inclusion of basalt fluid components.

Migrations in a seismic process are isolated by the analysis of three-dimensional spatial-temporal diagrams with axes: time, distance projection and energy parameter – decimal logarithm of total emitted earthquake energy ( $\lg E_{\text{sum}}$ ), obtained for projection areas of seismic data. The symmetry axis of projection areas is aligned with the direction of elongated epicenter concentrations. The width and length of the projection area are determined according to the size of the epicenter concentrations (see Fig. 1).

The parameter  $\lg E_{\text{sum}}$  was calculated using data of the Baykal Regional Seismological Center, Geophysical Survey of the Russian Academy of Sciences (BRSC GS RAS 2019). The energy of earthquakes was summed up over a period of time  $\Delta T=1$  month within projection cells  $\Delta L=0.1^\circ$ . In each unit cell, the total energy was calculated as the sum of the energy of all earthquakes:

$$\lg E_{\text{sum}} = \lg \left( \sum_{i=1}^n E_i \right)$$

where  $n$  is the number of seismic events in the cell,  $E$  is the energy of earthquakes in Joules, calculated as  $E=10^K$ , where  $K=4+1.8M$  is the energy class of events (Rautian et al. 2007), and  $M$  is the magnitude of the earthquakes ( $2.0 \leq M < 7.3$ ). The spatio-temporal diagram of the  $\lg E_{\text{sum}}$  was created by the MathGL program (MathGL 2019) using dataset for the instrumental period of between the years 1964–2002 for representative earthquakes (energy class  $K \geq 8$ ). The diagram shows the  $\lg E_{\text{sum}}$  values interpolated within the spatiotemporal window  $3\Delta T \times 3\Delta L$  by linear interpolation. The  $\lg E_{\text{sum}}$  scale reflects the values smoothed in this window. Smoothing of the space-time matrix is performed for more convenient visualization, when closest clusters of total energy are combined into chains. The slope of energy clusters chains

in the spatial-temporal diagram reflects the velocity and direction of seismic activity propagation. To determine the velocity of seismic activity migration, the ratio of the distance projection (in km) to the time projection (in years) is used.

## Results

### ***The distributions of thermal springs and earthquake swarms by the fault density***

Figure 1 shows that in a small scale, the hydrotherms are associated with large maxima, while swarms of earthquakes are located, systematically, between areas of hydrotherms concentration. A more detailed analysis of the fault density network allows to see that the maxima of fracturing areas are located on the sides of the depressions, at isthmuses between depressions, somewhere including the bordering parts of the depressions.

The histogram of the distribution of cell's number for each  $n$  value for the cell size  $0.37^\circ \times 0.37^\circ$  is shown in figure 2a. Subsequently, in figure 2b, c, d, histograms of the hydrotherms and number of swarms in cells distribution for this cell size are reported.

The coefficient of variation of hydrothermal springs quantity (in cells) samples is  $V=43\%$ ; for a sample of earthquake swarms in cells  $V=44\%$ , which is about 10% higher than the low uncertainty threshold values of  $V=33\%$ . It causes some uncertainties in the results due to a deficiency of some data.

To analyze the resulting distributions for randomness and uncertainty, the autocorrelation functions were calculated. The correlation diagrams of the hydrothermal spring's (Fig. 3a) and number of swarms in cells distribution (Fig. 3b) have high autocorrelation coefficient values of the first ( $L=1$ ) and second ( $L=2$ ) orders in certain ranges of  $n$  values, which indicates a trend in the data, characterizing the distributions as being different from random noise, since the trend indicates a good dependence of the neighboring values of the distribution functions from each other. The values of the autocorrelation significance function for hydrotherms (Fig. 3c) exceed the Student coefficient ( $t$ ) threshold to density values 17–21, and for swarms 13–14 (Fig. 3d) (for  $t$  threshold of confidence level  $0.9 > p > 0.975$ ). Thus, it can be seen that the distribution of swarms is defined in a narrower range of parameters  $n$ , and the distribution of the thermal springs is wider.

In general, the number of thermal springs without earthquake swarms into the cells is 38, and the number of springs in cells with swarms is 20, which is 2 times less (Fig. 2d). This ratio reflects the weak spatial correlation of the springs and earthquake swarms during the primary visual analysis. But at the range of  $n$  10–15, the ratio of thermal springs and earthquake swarms is other (Fig. 2d, c): the number of thermal springs in cells with swarms is 19, and without swarms - 15.

The largest number of swarms is associated with cells of  $n=13$ . The distribution of the swarm frequency positions into the cell by the density of faults is given in Tab. 1. At the density range below the average value of  $n$ , the number of swarm is 27%, and the number of thermal springs is 16 %;

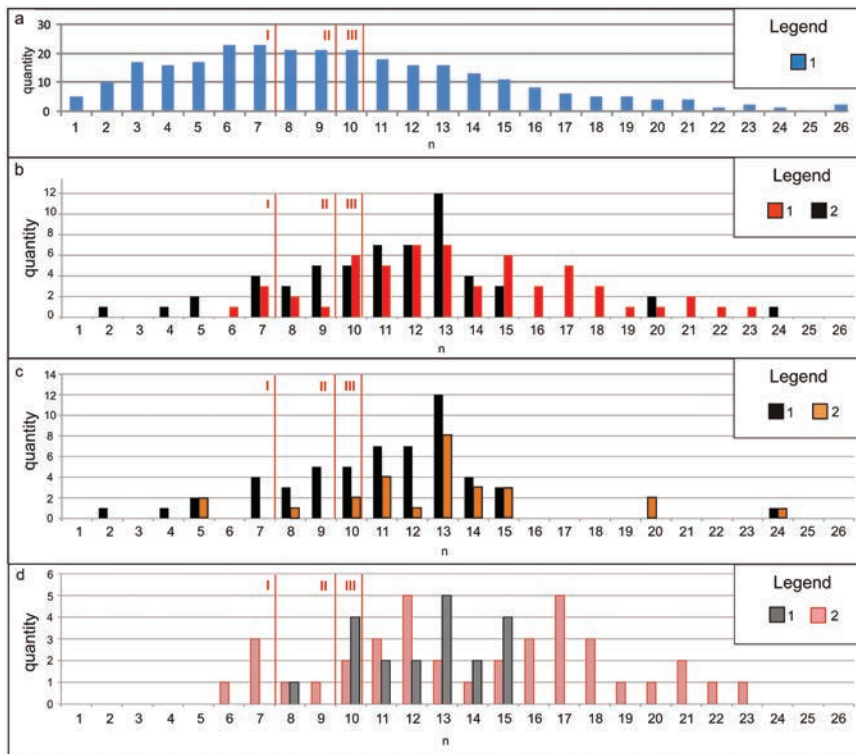


Fig. 2 - Histograms of the earthquake swarms and hydrothermal springs distribution by the parameter  $n$ : a - distribution of pallet cells  $0.37^\circ \times 0.37^\circ$  number by  $n$ ; b - the ratio of the swarms number getting inside cells (1) and the thermal springs quantity (2); c - the ratio of the total number of swarms in each cell (1) with the number of swarms getting inside cell with thermal springs (2); d - the ratio of the thermal springs quantity in cells with swarms (1) and the thermal springs quantity in cells without swarms (2). I - modal ( $n=7$ ); II - median ( $n=9$ ) and III - average ( $n=9.8$ ) fault density values ( $n$ ).

Fig. 2 - Istogrammi dello sciame sismico e della distribuzione delle sorgenti idrotermali secondo il parametro  $n$ : a - distribuzione di gruppi di celle  $0.37^\circ \times 0.37^\circ$  numerate da  $n$ ; b - il rapporto tra il numero di sciami all'interno delle celle (1) e la quantità di sorgenti termali (2); c - il rapporto tra il numero totale di sciami in ciascuna cella (1) e il numero di sciami che si trovano all'interno di una cella con le sorgenti termali (2); d - il rapporto tra la quantità di sorgenti termali nelle celle con gli sciami (1) e la quantità di sorgenti termali nelle celle senza gli sciami (2).

I - modale ( $n=7$ ); II = mediana ( $n=9$ ) e III = media ( $n=9.8$ ) dei valori di densità delle faglie ( $n$ ).

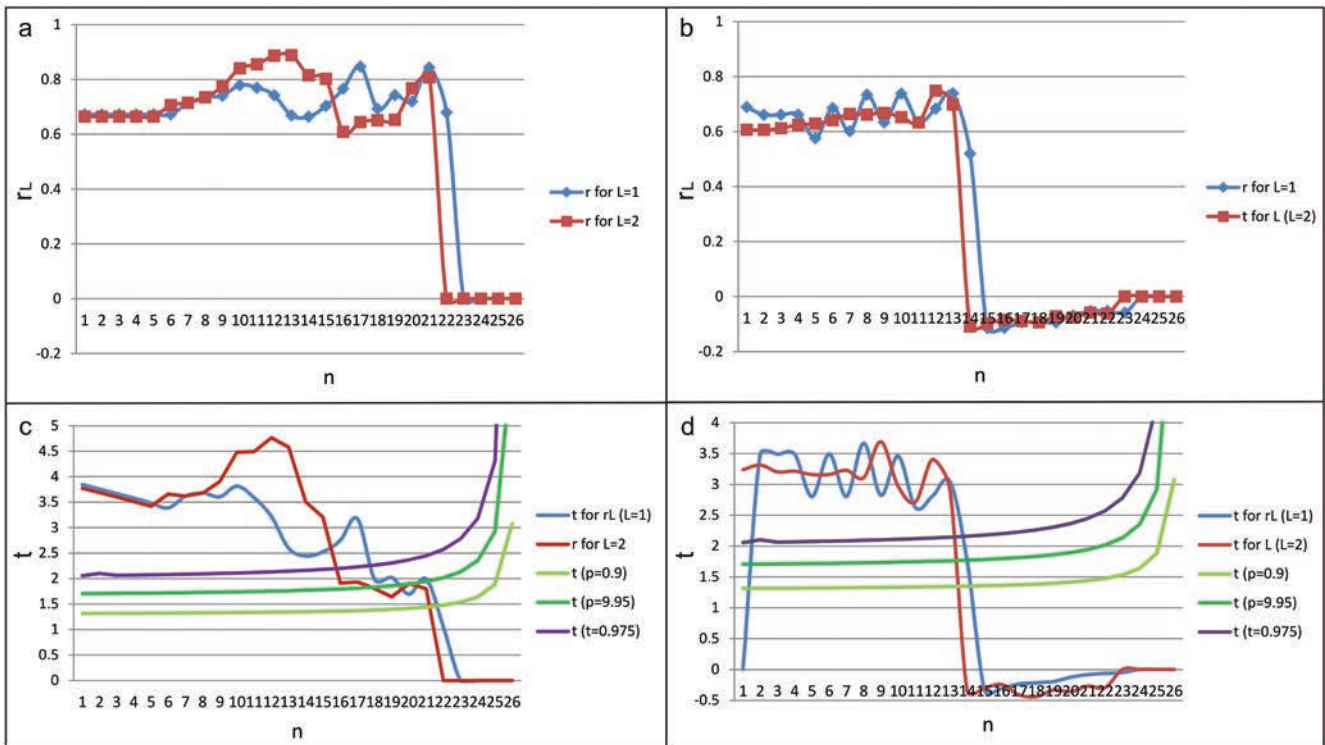


Fig. 3 - Autocorrelation functions of the first (offset  $L=1$ ) and second ( $L=2$ ) orders of hydrothermi's number distribution (a), and of earthquake swarms' number distribution (b). The respective significance functions of autocorrelation coefficients and significance thresholds for for correlograms of figure 3, a (c), and of figure 3, b (d) (Student coefficients  $t$  for different levels of confidence:  $p=0.9$ ,  $p=0.95$ ,  $p=0.975$ ).

Fig. 3 - Funzioni di autocorrelazione del primo (offset  $L=1$ ) e secondo ( $L=2$ ) ordine relative alla distribuzione del numero di sorgenti idrotermali (a) e degli sciami sismici (b). Il rispettivo significato delle funzioni dei coefficienti di autocorrelazione e le soglie di significatività per i correlogrammi di figura 3, a (c), e di figura 3, b (d) (coefficiente  $t$  di Student per diversi livelli di confidenza:  $p=0.9$ ,  $p=0.95$ ,  $p=0.975$ ).

above the average value of  $n$  the number of swarms is 72%, and that of thermal springs is 84%. The distribution modes of hydrotherms and swarms intersect in a narrow range of  $n$  value about 13 (Fig. 2b, c, d). Analysis of distributions shows that swarm events are associated with a less broken space of earth's crust consolidated blocks (Fig. 2b), and the hydrotherms are connected also with a more fractured space (Fig. 2b). The narrower localization of swarms than of hydrotherms (Tab. 1, Fig. 2b) indicates that the swarms are close to the borders of earth's crust consolidated blocks. This area of elevated quantity of faults (above the average value of  $n$ , but not the maximum value) is characterized by a high activity of the subsoil. There is a direct linear correlation with the correlation coefficient  $r=0.79$  between the values of the heat flux and the probable strength of the earthquake (Pinneker et al. 1984). Also, previously, we established an inverse correlation dependence of the hydrothermal water temperature and the density of faults (Novopashina and Kuz'mina 2018). Accordingly, in general, the thermal springs associated with the same density range as the swarms of earthquakes are hotter than the hydrotherms of the more fractured medium. These are mostly hot and warm springs. It also emphasizes the big depth of active faults associated with earthquake swarms.

The considered distribution of strong ( $4.7 \leq M < 6.8$ ) and very strong ( $6.4 \leq M < 7.3$ ) earthquakes shows that only 20% of strong earthquakes fall into the cells with thermal springs, and these are weaker events.

In general, the strong and the very strong events occur more often in areas of density below the average value of  $n$  (Tab. 1). These are the areas of the bridges between the depressions and the active fault's segments that are part of the lithosphere destruction zone.

Tab. 1 - Percentage distribution of thermal springs, strong earthquake and earthquake swarms number by the density of active faults ( $n$ ).

Tab. 1 - Distribuzione percentuale delle sorgenti termali, dei terremoti forti del numero di sciami sismici secondo la densità delle faglie attive ( $n$ ).

Parameter $n$	Less than 5	6–9	10–13	14–17	18–21	22–25
Thermal springs	0	16	32	29	18	5
Earthquake swarms	7	21	54	12	4	2
Strong earthquakes	0	44	17	17	17	6

### Fluid saturation state and rheological lithosphere properties in the zones of thermal water outlets allocation

Along the depressions sides, an area of tectonic activity is allocated with a specific density of faults, characterized by the maximum number of hydrothermal and swarm activity in figure 2b, c, d, where the distribution modes of the swarms and hydrotherms superimpose. The active faults of the northeastern part of the Baikal rift system, which

divide into parts the blocks of the earth's crust, are deep, and in the database of active faults (Lunina 2016) are listed as strike faults and strike-slip faults with a depth of more than 35 km. The results of the hydrothermal waters chemical composition analysis of the Barguzin depression area, using the methods of physico-chemical modeling, show that the contents of chemical elements: fluorine F, chlorine Cl, sulfur S, in water of the nitrogen hydrotherms Umhei, Seyuy, Alla (Fig. 5a) are not provided only by host rock (such as granites, sands, silts, muds) (Tab. 2). Despite of mainly infiltration genesis of thermal spring's water, only the addition of basalt fluid components to the physico-chemical model, obtained using the program "Selector", gives the convergence of the observed contents with the model data (Tab. 2). However, the basaltic fluid can exist at a depth of geoisotherm 1100 °C and more. This temperature corresponds to the lithosphere-asthenosphere boundary and below (more than 70 km), so there should be flexures in the upper mantle, which could be the paths of entering of chemical elements, coming from asthenosphere to the upper part of the lithosphere. Along with a high pressure gradient, the seismic process can facilitate the vertical migration of these elements.

Tab. 2 - Results of modeling in the system "host rocks and basalt fluid".

Tab. 2 - Risultati della modellazione nel sistema "host rock and basalt fluid".

Name of thermal spring	Element	Measured value of molar concentration (molality), mole/L	Model value of molality in model without basalt fluid components, mole/L	Model value of molality in model with basalt fluid components, mole/L
Umhei	F	$7.54 \cdot 10^{-4}$	$2.37 \cdot 10^{-5}$	$8.18 \cdot 10^{-4}$
	Cl	$1.02 \cdot 10^{-3}$	$2.23 \cdot 10^{-6}$	$1.00 \cdot 10^{-3}$
	S	$8.98 \cdot 10^{-4}$	$4.02 \cdot 10^{-6}$	$9.03 \cdot 10^{-4}$
Seyuy	F	$9.54 \cdot 10^{-4}$	$2.21 \cdot 10^{-5}$	$9.69 \cdot 10^{-4}$
	Cl	$3.78 \cdot 10^{-4}$	$2.08 \cdot 10^{-6}$	$4.02 \cdot 10^{-4}$
	S	$6.29 \cdot 10^{-4}$	$3.75 \cdot 10^{-6}$	$4.30 \cdot 10^{-4}$
Alla	F	$6.07 \cdot 10^{-4}$	$1.11 \cdot 10^{-6}$	$6.06 \cdot 10^{-4}$
	Cl	$7.58 \cdot 10^{-4}$	$1.04 \cdot 10^{-6}$	$8.01 \cdot 10^{-4}$
	S	$5.76 \cdot 10^{-4}$	$1.88 \cdot 10^{-6}$	$6.01 \cdot 10^{-4}$

Filtration links from the surface zone to the deeper layers occur through deep faults, thus areas far from faults are characterized by a difficult water exchange between the deep layers and the surface (Fig. 4). The watering of the Earth's crust deep zones and transit zones is clearly visible in the geoelectrical section of the Earth's crust (Fig. 4). In the section of the northeastern part of the BRS, the following layers are defined by deep magnetotelluric sounding (Pospeev 2012) (Fig. 4).

The roof of the conducting asthenospheric layer is visible at a depth of 70–80 (layer I in Fig. 4), as well as determined in a seismic section (Vinnik et al. 2017) and by the gravimetric method (Petit and Déverchère 2006). Basalt fluid, probably

existing in this zone as a result of partial mantle matter melting, at temperatures from 1100° C and higher, can be a source of such chemical elements as hydrogen, fluorine, chlorine and sulfur, which play a big role in geodynamic processes. .

Above the asthenosphere layer there is a non-conductive layer of the upper mantle with upper bound at a depth of 35–42 km (layer II in Fig. 4), where brittle deformations are almost not fixed. The high electric resistance of this layer indicates a dry state of matter at this depth. Nevertheless, it is in a more plastic state than the upper fragile layers due to temperature and pressure.

The root parts of the faults at this depth are assumed to be flexures, drain this layer, carrying out the gas phase of simple compounds.

Further along the section, the conducting layer extends to the Conrad border, located at a depth of 10–20 km (layer III in Fig. 4). The conductivity of this layer is most likely related to water saturation. Water in this layer can be released as a result of active reduction of trivalent iron oxides by hydrogen coming from the lower layers (Letnikov 2006) when the

geoisotherm reaches 800–900° C. ). This layer is characterized by the least amount of earthquakes due to the stress relaxing properties of the water containing environment.

At the roof of this layer, where the temperature reaches 350° C (approximately at the border of Conrad) in the granitization zone, the processes of amphibolization are started, where the water, formed in the conducting layer, is taken by metamorphic rocks (amphiboles and micas), forming a screen of low permeability and prevents further migration of water fluid to the top, therefore, a layer in the range from 5–20 km to 3–5 km is not fluid-saturated and has a high total electrical resistance. Most of the earthquake foci are concentrated in this zone (Radziminovich et al. 2013), since fragile properties of this layer are enhanced, and the relaxing ones are reduced. The aqueous fluid permeability of this layer is provided mainly by active conductive faults, as a drainage system, which allows fluids of the lower crustal layer to penetrate closer to the surface layers without undergoing significant transformations (water reacts with granites with low intensity). The faults are visible in the geoelectrical section as vertical zones of low resistance (Seminsky and Tugarina 2012).

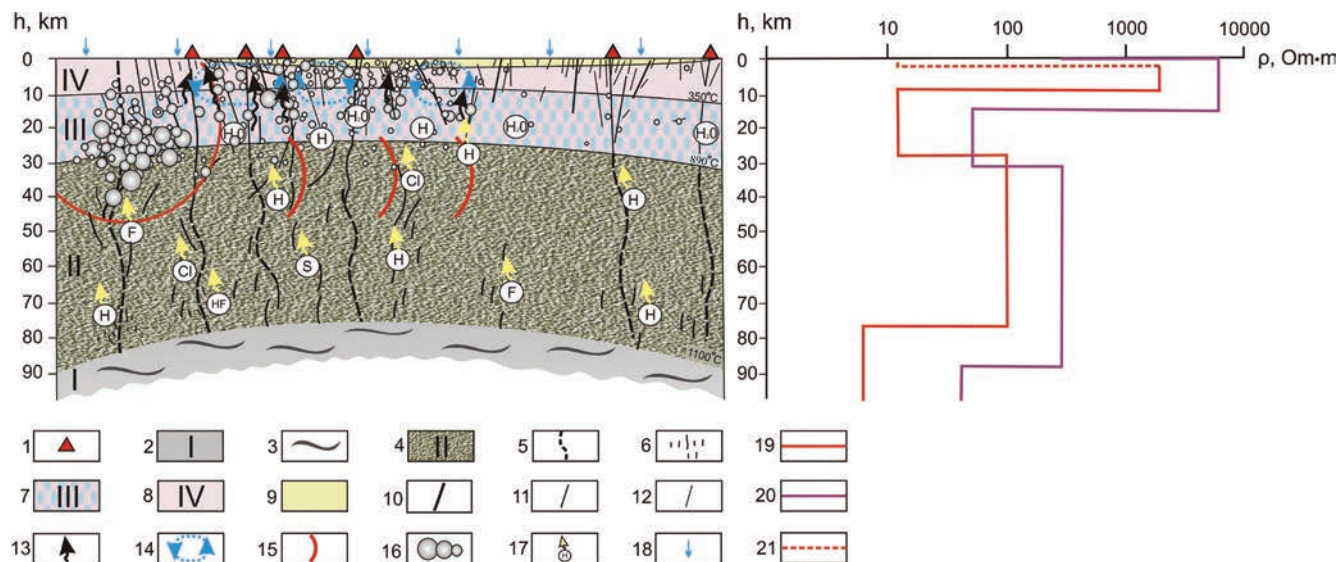


Fig. 4 - Provisional physico-geological model of the Earth's crust – upper mantle structure along the seismic migration trend direction (northeast-southwest direction), using the rheological model of the lithosphere by Sherman (2005). The Barguzin depression (along the Barguzin fault) as the example is used. 1 – hydrothermal springs; 2 – asthenosphere layer I (plastic state) according to Petit and Déverchère (2006); 3 – basalt fluid; 4 – non-conductive layer II of the upper mantle (quasi-plastic state); 5 – assumed flexures; 6 – tectonites; 7 – conductive layer III of the lower crust (quasi-brittle destruction); 8 – layer IV of high resistance (brittle destruction, granite batholith); 9 – Quaternary sediments of depression; 10 – deep active faults of depression sides; 11 – second order faults; 12 – near-surface active faults; 13 – water fluid; 14 – convection cells; 15 – deformation front; 16 – earthquakes of different energy; 17 – gases defusing from the asthenosphere and upper mantle along the deep faults of the depression sides; 18 – atmospheric water; 19 – electrical resistance graph of the depression area of the northwestern BRS part (Pospeev 2012); 20 – electrical resistance graph of the elevated area of the northwestern BRS part (Pospeev 2012); 21 – assumed electrical resistance value of the sedimentary layer (Seminsky and Tugarina 2011) according to EV Pospeeva, Trofimuk Institute of Petroleum-Gas Geology and Geophysics of the Siberian Branch of the RAS.

Fig. 4 - Modello fisico-geologico provvisorio (?) della crosta terrestre-struttura del mantello superiore lungo il trend di migrazione sismica (direzione nord est-sud est), ottenuto usando il modello reologico della litosfera di Sherman (2005). La depressione di Barguzin (lungo la faglia di Barguzin) dove è stato applicato l'esempio; 1- sorgenti idrotermali; 2 strato dell'astenosfera I (stato plastico) in accordo con Petit eDeverchere (2006); 3 – fluido basaltico; 4- strato II non conduttivo del mantello superiore (stato quasi-plastico); 5- pieghe assunte; 6- tettoniti; 7- strato III conduttivo della crosta basale (fratturazione semi-fragile); 8- strato IV ad alta resistenza (fratturazione fragile, graniti a batoliti); 9- sedimenti quaternari delle depressioni; 10- faglie attive profonde ai fianchi delle depressioni; 11- faglie di secondo ordine; 12 – faglie attive superficiali; 13 - fluidi acquosi; 14 - celle di convezione; 15 - fronte di deformazione; 16 - terremoti di differente intensità; 17 - defusing dei gas dall'astenosfera e dal mantello superiore lungo le faglie profonde delle aree depresse; 18 - acqua atmosferica; 19 - grafico della resistenza elettrica dell'area della depressione della parte nord est di BRS (Pospeev 2012); 20 - grafico della resistenza elettrica dell'area in alto della parte nord est di BRS (Pospeev 2012); 21 - valore assunto della resistenza elettrica dello strato sedimentario (Seminsky and Tugarina 2011) in accordo con EV Pospeeva, Trofimuk Institute of Petroleum-Gas Geology and Geophysics della Sezione Siberiana del RAS.

Thus, deep faults serve as the main drain between the upper part of the section and the mantle, and fault structures of lower order contribute to the circulation and transit of aqueous fluid in the fragile part of the section in a layer of 5–10–10–20 km. Horizontal and vertical structural heterogeneity of the lithosphere causes heterogeneous of watering, that probably influence on the processes of triggering, relaxation and propagation of the seismic process.

Based on the idea that conductive water-flooded zones are tectonic stress unloading zones, and more “dry” non-conductive zones are zones of brittle deformations, and also taking into account the spatial arrangement of drainage fault zones, the conceptual model shown in figure 4, has been compiled, also using the rheological lithosphere model proposed by Sherman SI (2005). The figure shows that strong shocks of an earthquake swarm (the Amut swarm was taken as an example), which occurred at a considerable depth, are the source of a deformation front propagating in various directions.

### **Seismic activity propagation in zones of high fracture and hydrothermal activity**

Today, there is the conception of aqueous fluid's participation in seismic activity migration accompanying the process of horizontal and vertical interaction, both between different lithosphere layers and the upper mantle and lower-crustal layers (Chéry et al. 2001; Bürgmann and Dresen 2008; Becken et al. 2011; Kariche et al. 2018; Jónsson et al. 2002; Marone et al. 1991; Tung and Masterlark 2018; Tung et al. 2018).

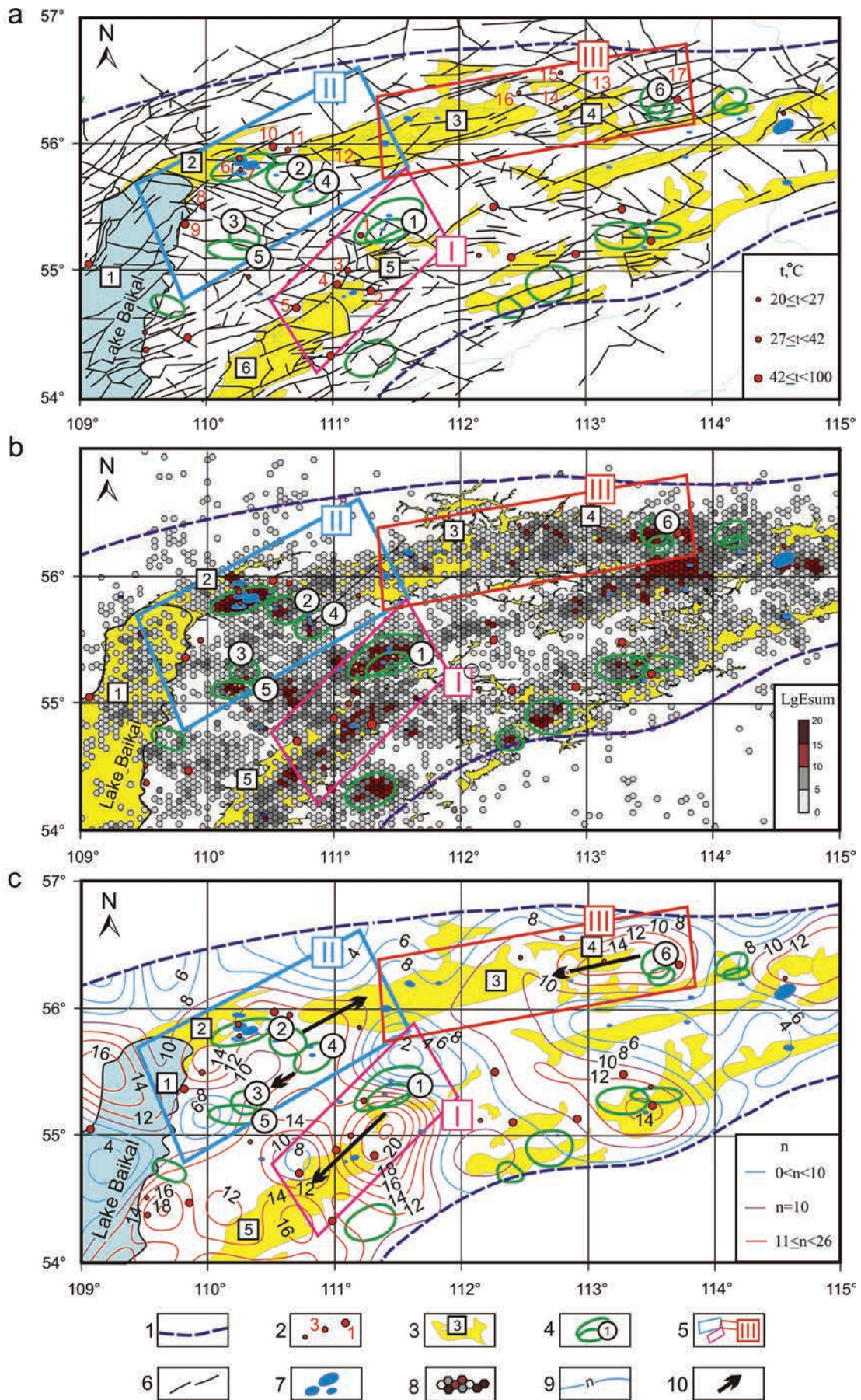
In order to see how the seismic process develop over the time in the earth's crust of different fracture level and how it relates to the location of the thermal springs, spatial-temporal diagrams for some linear tectonic structures of northeast orientating areas (Fig. 5) were analyzed, which are marked by concentrations of earthquake epicenters of different forces (Fig. 5a, b). Along such zones of released seismic energy, the seismic data projection areas were set, covering fault density maxima, concentration of epicenters and earthquake swarms (Fig. 5b, c).

In areas of increased fracturing (n), such as sides of the Barguzin, Kichera, Verkhneangara depletions, which are characterized by hydrotherms concentration, migrations of seismic activity are recorded. They are sequences of seismic energy clusters including weak and moderate seismic events. At the edge of such migration chains there are strong seismic events. For example, the Amut earthquake swarm of 1979–1980, including strong seismic events ( $M \geq 5$ ), occurred at the border between the maximum and minimum values of parameter n (Fig. 1, Fig. 5a). Multiple sequences of moderate and weak seismic events, traced in a spatial time diagram from a swarm, are recorded in direction from northeast to southwest. In the figure 6a the spatial-temporal diagram of parameter  $LgE_{sum}$  for the Amut swarm region for the period between the years 1964–2010 is presented. The diagram is obtained for the seismic data projection zone I in figure 5. The diagram shows the trend of directional propagation of seismic energy from a cluster of main shakes for the years 1979–1981 in the south-west direction over a distance of 110 kilometers along the Barguzin strike fault during 22 years, which corresponds to a velocity of about 5 km/year. Against the background of the main trend, higher-velocity (10–40 km/year) multidirectional chains of seismic energy maxima are observed. In the first two years during the period (1980–1982) an ordered sequence of weak and moderate events propagation at the velocity of 20–25 km/year is observed (yellow dotted ellipse I in Fig. 6a), which then changes the propagation vector to the opposite direction (ellipse II, III in Fig. 6a). Such multidirectional chains marks back-forward propagation episodes of earth's crust deformations along separate fault zones – along active segments smaller than total lithosphere destruction zone. The seismic energy migration area corresponds to the area of maximally fractured space and concentration of the following hydrothermal springs: Alla, Kuchiger, Umhey, Megdylkon, Seyuy.

Diagram for the seismic data projection area II (in the Fig. 5) is presented in the Fig. 6b. Zone II includes Kumor earthquake swarm happened in the period 1966–1967. The diagram shows the seismic process distribution (yellow

Fig. 5 next page - Zones of seismic data projection (data collection) by the Baikal Branch of the Geophysical Survey (BRSC GS RAS 2019), including the earthquake swarms areas and areas of thermal springs concentrations. a - map of active faults (Lunina 2016); b - map of the total energy of earthquakes  $LgE_{sum}$  (data display period is 1974–2010 years); c - map of the active faults density for the  $0.37^\circ \times 0.37^\circ$  cell size. 1 - the BRS contour; 2 - thermal springs with their numbers marked with red text (1 - Meghdylkon, 2 - Seyuy, 3 - Umhey, 4 - Kuchiger, 5 - Alla, 6 - Korikei, 7 - Verkhnyaya Zaimka, 8 - Frolikha, 9 - Khakusy, 10 - Jilinda, 11 - Kiron, 12 - Irkana, 13 - Turikan, 14 - Verkhneangara, 15 Churin, 16 - Sartin, 17 - Verkhneangarakan);  $20^\circ C < t < 37^\circ C$  (warm, little red circle);  $4 - 37^\circ C < t < 42^\circ C$  (hot, medium red circle);  $42^\circ C < t < 100^\circ C$  (very hot, big red circle); 3 - the BRS depressions with their numbers in the squares (1 - Baikal, 2 - Kichera, 3-4 - Verkhneangara, 5 - Amut, 6 - Barguzin); 4 - swarms of earthquakes with their numbers in circles (1 - Amut 1979–1981, 2 - Kumor 1966–1967, 3 - Verkhnetompudin 1971, 4 - Svetlin 1976–1978, 5 - Srednetompudin 1975, 6 - Angarakan 1979–1081); 5 - zones of seismic data projection with their numbers (Roman numerals in squares); 6 - active faults of the BRS; 7 - earthquakes foci projections of magnitude  $M > 5$ ; 8 - hexagonal cells highlighted in color depending on  $LgE_{sum}$ ; 9 - fault density contour lines for a pallet  $0.37^\circ \times 0.37^\circ$ ; 10 - directions of seismic activity migration front.

Fig. 5 pagina a fianco - Zone di proiezione dei dati sismici (raccolta dati) dalla sezione del Geophysical Survey del Baikal (BRSC GS RAS 2019), incluse le aree degli sciami sismici e le aree di concentrazione delle sorgenti termali. a- carta delle faglie attive (Lunina 2016); b- carta dell'energia totale dei terremoti  $LgE_{sum}$  (periodo di visualizzazione dei dati è dal 1974 al 2010); c- mappa di densità delle faglie attive per la dimensione delle celle  $0.37^\circ \times 0.37^\circ$ . 1 - limite del BRS; 2 - sorgenti termali con numeri indicati in rosso (1 - Meghdylkon, 2 - Seyuy, 3 - Umhey, 4 - Kuchiger, 5 - Alla, 6 - Korikei, 7 - Verkhnyaya Zaimka, 8 - Frolikha, 9 - Khakusy, 10 - Jilinda, 11 - Kiron, 12 - Irkana, 13 - Turikan, 14 - Verkhneangara, 15 Churin, 16 - Sartin, 17 - Verkhneangarakan);  $20^\circ C < t < 37^\circ C$  (molto calde, indicate con pallino rosso piccolo);  $37^\circ C < t < 42^\circ C$  (molto calde, indicate con pallino rosso medio);  $42^\circ C < t < 100^\circ C$  (bollenti, indicate con pallino rosso grande); 3 - le depressioni BRS con i loro numeri nei quadrati (1 - Baikal, 2 - Kichera, 3-4 - Verkhneangara, 5 - Amut, 6 - Barguzin); 4 - sciami sismici con i loro numeri nei cerchi (1 - Amut 1979–1981, 2 - Kumor 1966–1967, 3 - Verkhnetompudin 1971, 4 - Svetlin 1976–1978, 5 - Srednetompudin 1975, 6 - Angarakan 1979–1081); 5 - zone di proiezione dei dati sismici con i loro numeri (Numeri Romani nei quadrati); 6 - faglie attive nel BRS; 7- proiezioni degli epicentri dei terremoti di magnitudo  $M > 5$ ; 8 - celle esagonali evidenziate a colori a seconda del  $LgE_{sum}$ ; 9 - linee di contorno di densità di faglie per gruppi  $0.37^\circ \times 0.37^\circ$ ; 10 - direzione del fronte di migrazione dell'attività sismica.



dotted ellipse 1 in the Fig. 6b) towards south-west in the region of elevated values of parameter  $n$  towards the swarms: Verkhnetompudin (1971) and Srednetompudin (1975), and then by the opposite direction. Those parts of the seismic data projection zone II, where the seismic activity migration front is recorded, include the thermal springs: Kyron, Geelinda, Korikei, Verhnyia Ziamka. The other branch of seismic energy migration has a northwest direction (dotted ellipse II in Fig. 6b), includes the Irkan hydrothermal spring and runs to the area of fault density values above the average value. In the lowest sector of the diagram b in figure 6 the Frolikha and Khakusi springs are located close to the Verkhnetompudin and Srednetompudin swarms, where the heat flow maxima are observed (see Fig. 1). About 10 years later, in the area of the

Kumor earthquake swarm, the Svetlin swarm occurs, which causes branches of seismic activity migrations similar to the chains of the Kumora swarm.

The diagram for the projection area III of figure 5 is reported in figure 6c. In the upper sector of diagram the the Angarakan swarm area is highlighted in the period 1979–1983. The Verhneangarakan thermal spring is located in this zone. Multiple seismic activity migrations of different directions are visible here. Clearly visible migration chains are highlighted with ellipses I, II in figure 6c.

From the Angarakan swarm, seismic activity propagate through the fractured area (ellipses II, III in Fig. 6c), where the thermal springs: Turikan, Churin, Verkhneangara are located. The middle part of the diagram c of the figure 6 corresponds

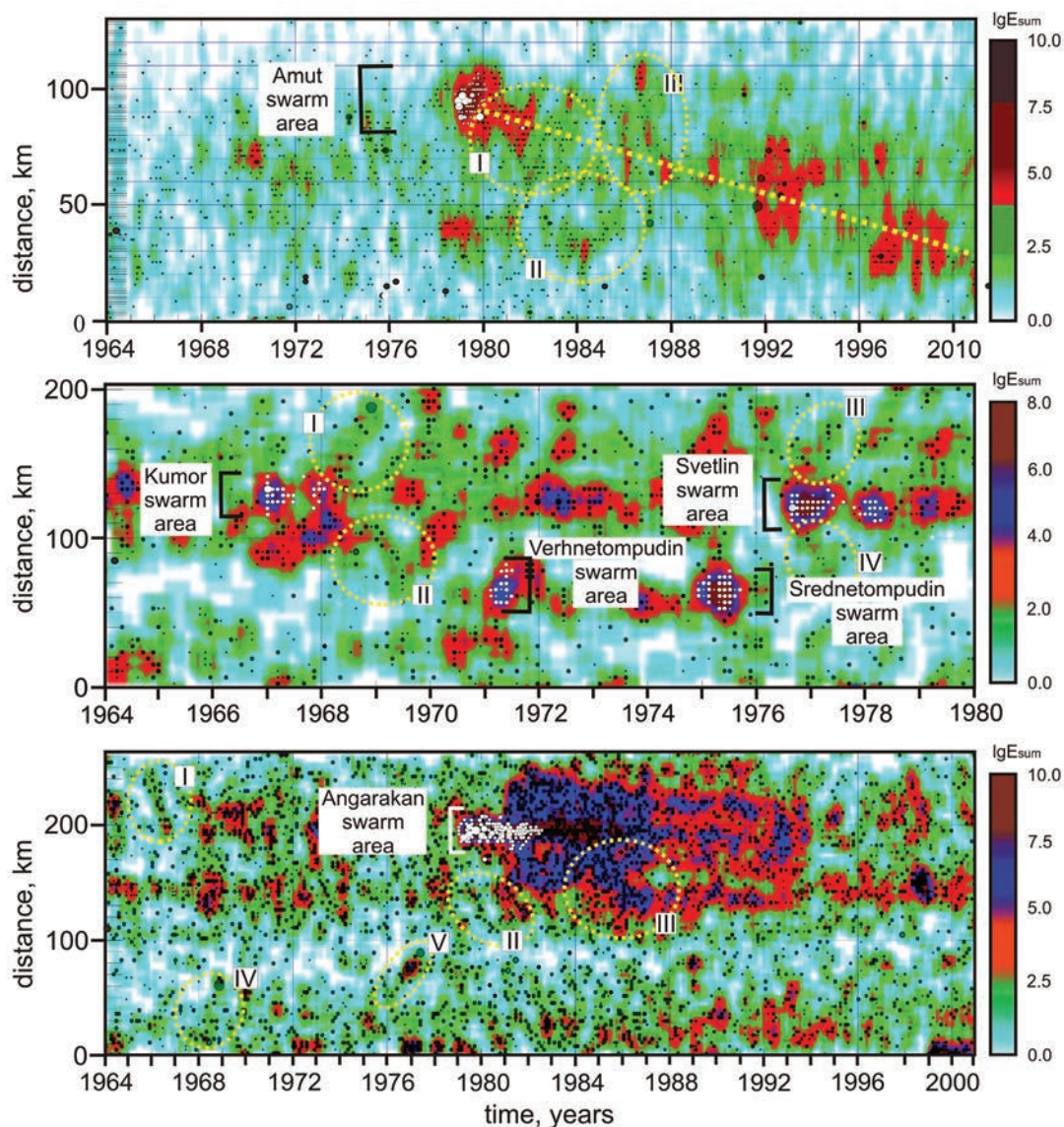


Fig. 6 - Spatial-temporal diagrams for projection zones of seismic data shown in figure 1 and figure 5: for zone I (a) from Novopashina AV Kuz'mina (2017), for zone II (b), for zone III (c). The diagram is plotted by the MathGL software (2019). The diagram consists of two layers: the layer of interpolated  $LgE_{sum}$  values (color) is covered by the layer of seismic event points.

Fig. 6 - Diagrammi spazio temporali per le zone di proiezione dei dati sismici mostrati in figura 1 e figura 5: per la zona I (a) da Novopashina AV Kuz'mina (2017), per la zona II (b), per la zona III (c). Il digramma è realizzato con il programma MathGL (2019). Il digramma consiste in due livelli: il livello dei valori interpolati  $LgE_{sum}$  (colorato) sta sotto al livello dei punti degli eventi sismici.

to a less fractured area (low density values in Fig. 5c). Its boundaries are marked by events of magnitude  $M \geq 5$  (ellipses IV, V in Fig. 6c). These events complete the migration process of the lowest diagram sector, proceeding in a fractured zone and corresponds to the Irkana hydrothermal spring location (Fig. 5a). The diagram shows that strong events occur in the area of the bridge between two fractured zones, marking the stage of segments accretion of a larger fault zone. Thus, the migration of seismic energy proceeds in fractured areas with multiple manifestations of thermal outlets at value of  $n$  from 12–14 and higher.

## Discussion

Analyzing the whole quantity distribution of hydrothermal sources and earthquake swarms, it can be concluded that earthquake swarms occur 1.5 times less frequently in areas with thermal springs. This might be due to shifting of swarms distribution to a less fragmented space (but not too much as strong earthquakes), and to a shifting of the thermal springs distribution to a more fractured environment.

Hydrothermal springs and earthquake swarms are associated with faults, which separate the blocks of the earth's crust from the interblock space, penetrate below the crust-mantle boundary, which is indirectly confirmed by deep localization of hypocenters and by the results of physico-chemical modeling of the hydrothermal springs chemical composition formation of the Barguzin depression (Umhei, Seyuy, Alla): high contents of the elements F, Cl, S can be explained by the contribution of the components of the deep fluid.

In Becken et al. (2011), it was shown that the reason of seismicity stimulating and determining of seismic activity amplitude variations along strike is the migration of fluids from the lower crust and upper mantle to the weakened (fractional) zone with the lowest filtration resistance. Different layers of the lithosphere and upper mantle, with different rheological and physical properties, will respond differently to the coulomb tectonic stresses transfer changes. In the lower more plastic layers, the stresses will be transmitted slowly, transferring tectonic stress to the upper layers and causing the pore fluid pressure change in the upper layers: first in the watered conductive layer III, and then in the fractured collector of the non-conductive fragile layer IV (see Fig. 4). The fluid migration process upward along the section, caused by an increase in the tectonic stress, in the watering layer will be accompanied mainly by relaxation as few seismic events, and in fractured parts of fragile nonconducting layer the fluid movement will trigger a higher earthquake count, since high pore or fracture water pressure neutralizes the geostatic load and induces a reduction in effective stress value (Acosta et al. 2018), contributing to the relaxation of the tectonic stress (Pinneker et al. 1984). For this reason, the sequential propagation of the deformation front in the fractured zone resembles a sequence of weak and moderate events.

In the interblock zones, the lithosphere is characterized by a combination of the following conditions: lowered depth of more plastic layers of the upper mantle (layer II

in the Fig. 4), the presence of a fluid-saturated layer of the lower crust (layer III in the Fig. 4), the faults draining the earth's crust, a more broken layer of the upper crust (layer IV in the Fig. 4) and dispersed heat flow. All this probably lowers the total viscosity of the lithosphere in such zones, which creates suitable conditions for the stress transfer and relaxation, which is manifested in the seismic process by an ordered sequence of weak and moderate seismic events. Since swarms are located on the border of consolidated blocks, the consecutive propagation of the stress front occurs both toward the fractured zone and toward the solid crust blocks. Zones of high fracture and high amount of hydrothermal springs ( $12 \leq n \leq 17-21$ ), being an interblock space, are areas of tectonic stress unloading (Seminsky and Tugarina 2012), therefore, in the discharge area, the propagation of the stress front will be marked by chains of slow seismic activity migrations (Fig. 5: zones I, II, III, diagrams: 6a, 6b, the upper segment of the diagram 6c), and the propagation of the stress front towards consolidated blocks can be the cause of a strong seismic event or swarm (Fig. 5: zone III and the diagram in Fig. 6d, underside of the diagram). These processes are well traced in the seismic activity migrations observed of the Amut, Angarakan, Vernemetomudin, Srednemetpudin and Kychera swarms (Fig. 5).

Thus, if seismicity and water exchange are caused by the effect of seismic injection, this model describes the process of relaxation of tectonic stresses in accordance to a logical chain: seismic event – pore pressure rise of the rock – seismic event, etc. This process continues until the stress is completely relaxed or the spread of water is stopped by a kind of barrier, such as a low-permeable and denser consolidated crustal block with a reduced fault density that prevents water exchange.

## Conclusions

The fault density network structure reflects the Earth's crust heterogeneity of the Baikal rift system. Filtration connections of the surface zone with deeper layers occur along faults, and in areas distant from faults, drainage is weak, which prevents water exchange of these layers with the surface. The active faults framing the consolidated blocks, reaching the depths of the lower crust, upper mantle, and possibly the lithosphere-asthenosphere boundary (in the form of tectonites), can serve as transit zones for the entry of some chemical elements from the asthenosphere into the upper mantle and further up the section, as well as aqueous fluids from the lower crust to the upper part of the section, as evidenced by increased concentrations of such chemical elements as fluorine, chlorine, sulfur in the thermal waters.

The minimum faults density is related with consolidated blocks of the earth's crust, framed by deep regional faults, which are associated with earthquake swarms, high heat flux values, and rare thermal springs of high and medium temperatures. These block separation areas are zones of deep faults characterized by a density above the average value of  $n$ , but not the maximum. At the blocks boundaries, the distribution modes of thermal sources and earthquake swarms

coincide. Migration sequences start propagate through these zones.

Areas of higher fault density are zones of interblock space, characterized by fewer swarms of earthquakes, dispersed thermal field and by concentrations of multiple thermal springs. Migration sequences of seismic events of weak and moderate force propagate towards these zones.

The interaction of the raised upper mantle quasiplastic layer, responsible for the slow stress transfer front propagation, the lower crust layer and the upper thinned brittle layer of increased fracturing of interblock space, is accompanied by a pressure differential of fluids in pores and cracks.

Migration in a seismic process reflects the consistent interaction of seismicity and water fluid in the process of stress transfer from strong shocks included in earthquake swarms. Thus, zones of interblock space, maximum fracturing and concentration of hydrotherms, are the most likely areas of stress relaxation.

**Acknowledgment:** the authors are very grateful to Francesca Lotti, Emanuela Fusinato, Francesco La Vigna and for other reviewers and editors of the *Acque Sotterranee* journal for reviewing, remarks, valuable advices and correction on improving the article. Authors are also thankful to Robert Hanshaw and Christoph David Hohl for English proofreading.

## REFERENCES

- Artyushkov EV (1993) Physical tectonics. Moscow, Russia.
- Achtziger-Zupančič P, Loew S, Hiller A (2016) 3D fluid flow in fault zones of crystalline basement rocks (Poehla-Tellerhaeuser Ore Field, Ore Mountains, Germany). *Geofluids* 16:688–710. doi:10.1111/gfl.12192
- Acosta M, Passelègue FX, Schubnel A, Violay M (2018) Dynamic weakening during earthquakes controlled by fluid thermodynamics. *Nat Commun* 9:3074. doi:10.1038/s41467-018-05603-9
- Avchenko OV (2009) Fundamentals of physico-chemical modeling of mineral systems. Moscow, Russia.
- BRSC GS RAS (2019) Baykal Regional Seismological Center, Geophysical Survey of the Russian Academy of Sciences, Irkutsk, dataset of earthquakes for the period 1964-2002. Website: <http://seis-bykl.ru/> (last accessed on: 04.03.2019)
- Becken M, Ritter O, Bedrosian PA, Weckmann U (2011) Correlation between deep fluids, tremor and creep along the central San Andreas fault. *Nature* 480(7375):87–90. doi:10.1038/nature10609
- Boldina SV, Kopylova GN (2017) Effects of the January 30, 2016,  $m_w=7.2$  Zhupanovsky earthquake on the water level variations in wells yuz-5 and e-1 in Kamchatka. *Geodynamics & Tectonophysics* 8(4):863–880. (In Russ.) doi:10.5800/GT-2017-8-4-0321
- Bürgmann R, Dresen G (2008) Rheology of the lower crust and upper mantle: Evidence from rock mechanics, geodesy, and field observations". *Annu. Rev. Earth Planet. Sci.* 36:531–567. doi:10.1146/annurev.earth.36.031207.124326
- Chéry J, Merkel S, Bouissou S 2001 A physical basis for time clustering of large earthquakes. *Bulletin of the Seismological Society of America* 91(6):1685–1693. doi:10.1785/0120000298
- Chudnenko KV (2003) Selector - Windows software tool for calculating chemical equilibria minimizing thermodynamic potentials. Short instructions. Irkutsk, Russia.
- Deng K, Liu Y, Harrington RM (2016) Poroelastic stress triggering of the December 2013 Crooked Lake, Alberta, induced seismicity sequence. *Geophysical Research Letters* 43(16):8482–8491. doi:10.1002/2016GL070421
- Golubev VA (2007) Conductive and convective heat output in the Baikal rift zone. Novosibirsk, Russia.
- Freed AM (2005) Earthquake triggering by static, dynamic, and post-seismic stress transfer. *Annu. Rev. Earth Planet. Sci.* 33(3):35–67. doi:10.1146/annurev.earth.33.092203.122505
- Jónsson S, Zebker H, Segall P, Amelung F (2002) Fault slip distribution of the 1999 Mw 7.1 Hector Mine, California, earthquake, estimated from satellite radar and GPS measurements. *Bull. Seismol. Soc. Am.* 92:1377–1389. doi:10.3390/s150716786
- He J, Peltzer G (2010) Poroelastic triggering in the January 9–22, Nima-Gaize (Tibet) earthquake sequence. *Geology* 38(10):907–910. doi:10.1130/G31104.1,2010
- Hamling IJ, D'Anastasio E, Wallace LM, Ellis S, Motagh M, Samsonov S, Palmer N, Hreinsdóttir S (2014) Crustal deformation and stress transfer during a propagating earthquake sequence: The 2013 Cook Strait sequence, central New Zealand. *Journal of Geophysical Research: Solid Earth* 119(7):6080–6092. doi:10.1002/2014JB011084
- Heinicke J, Fisher T, Gaupp R, Götze J, Hoch U., Konietzky H, Stanel K-P (2009) Hydrothermal alterations a trigger mechanism for earthquake swarms: the Vegtland NW Bohemia region as a case study. *Geophys. J. Int* 178:1–3. doi:10.1111/j.1365-246X.2009.04138.x
- Hughes KLH, Masterlark T, Mooney WD (2011) Poroelastic stress-triggering of the 2005 M8.7 Nias earthquake by the 2004 M9.2 Sumatra–Andaman earthquake. *Lithosphere* 3:170–172. doi:10.1130/L109.1
- Ingebritsen S, Gleeson T (2017) Crustal permeability. *Hydrogeology Journal*. doi:10.1007/s10040-017-1663-4

- Ingebritsen SE, Shelly DR, Hsieh PA, Clor LE, Seward PH, Evans WC (2015) Hydrothermal response to a volcano-tectonic earthquake swarm, Lassen, California. *Geophys. Res. Lett.* 42:9223-9230. doi:10.1002/2015GL065826
- Kariche J, Timoulali Y, Meghraoui M, Cetin E, Toussaint R (2018) The Al Hoceima earthquake sequence of 1994, 2004 and 2016: Stress transfer and poroelasticity in the Rif and Alboran Sea region *Geophysical Journal International*. *Geophysical Journal International* 212(1):42-53. doi:10.1093/gji/ggx385
- Karpov IK (1981) Physico-chemical modeling by computer in geochemistry. Novosibirsk, Russia.
- Kazmin LA (1979) Calculation of chemical equilibria and refinement of thermodynamic constants by the method of minimization of the free energy in the system H<sub>2</sub>S–H<sub>2</sub>O. Novosibirsk, Russia.
- Kuzmina EA, Novopashina AV (2018) Groundwater outflows and fault density spatial relation in the Baikal rift system (Russia). *Acque Sotterranee - Italian Journal of Groundwater* AS24-324:51-60. doi:10.7343/as-2018-324
- Kuzmina EA, Veshcheva SV, Zarubina OV, Brianskii NV (2015) Un modello fisico-chimico come strumento per spiegare la composizione delle acque termali nelle regioni tettonicamente attive "Physico-chemical model as a tool to explain the composition of thermal waters in tectonically active regions". *Acque Sotterranee – Italian Journal of Groundwater* 13061:007–017. <https://doi.org/10.7343/as-109-15-0136>
- Letnikov FA (2006) Fluids in endogenic processes and problems of metallogeny. *Russian Geology and Geophysics* 47(12):1271-1281
- Levina EA, Ruzhich VV (2015) The seismicity migration study based on space-time diagrams. *Geodynamics & Tectonophysics* 6(2):225–244. doi:10.5800/GT-2015-6-2-0178
- Lin J, Stein RS (2004) Stress triggering in thrust and subduction earthquakes, and stress interaction between the southern San Andreas and nearby thrust and strike-slip faults. *Journal of Geophysical Research* V109(B02303). doi:10.1029/2003JB002607
- Lunina OV (2016) The digital map of the Pliocene-quaternary crustal faults in the southern east siberia and the adjacent northern Mongolia. *Geodynamics & Tectonophysics* 7(3):407-434. doi:10.5800/GT-2016-7-3-0215
- Lysak SV (2002) Heat flow in the zones of active faults in the south of Eastern Siberia. *Russian Geology and Geophysics* 8:791–803
- Marone CJ, Scholz C, Bilham R (1991) On the mechanics of earthquake afterslip. *Journal of Geophysical Research* 96(B5):8441-8452
- MathGL (2019) A library for scientific data visualization. Website: <https://sourceforge.net/projects/mathgl/reviews> (last accessed on: 05.03.2019)
- Matz VD, Ufimtsev GF, Mandelbaym ML, Alakshin AM, Pospeev AV, Shimarev ML, Khalilov OM (2001) Cenozoic of the Baikal rift depression: structure and geological history, Geo, Novosibirsk, Russia.
- Melnikova VI, Radziminovich NA, Chipizubov AV, Dobrynina AA, Gileva NA (2007) Activation of rifting processes in the Northern Cis-Baikal region: A case study of the Kichera earthquake sequence of 1999. *Izvestiya. Physics of the Solid Earth*. 43(11):905-921. doi:10.1134/S1069351307110018
- Novopashina AV, Kuzmina EV (2017) Earth's Crust Faults Density and Thermal Springs in the Seismic Activity Migration Zone at the Amutsky Swarm Region". *The Bulletin of Irkutsk State University. Series «Earth Sciences» (Izvestiya Irkutskogo gosudarstvennogo universiteta. Seriya «Nauki o Zemle»)*. 20:81–90.
- Novopashina AV, Sankov VA (2018) Migrations of released seismic energy in various geodynamic conditions. *Geodynamics & Tectonophysics* 9(1):139-163. doi:10.5800/GT-2018-9-1-0342
- Parotidis M, Rothert E, Shapiro SA (2003) Pore-pressure diffusion: A possible triggering mechanism for the earthquake swarms 2000 in Vogtland/NW-Bohemia, central Europe. *Geophys. Res. Lett.* 30(20):20-75. doi:10.1029/2003GL018110
- Passelègue FX, Brantut N, Mitchell Th M (2018) Fault reactivation by fluid injection: Controls from stress state and injection rate. *Geophysics*. arXiv preprint arXiv:1809.06652
- Pedretti D, Russian A, Sanchez-Vila X, Dentz M (2016) Scale dependence of the hydraulic properties of a fractured aquifer estimated using transfer functions. *Water Resources Research*. doi:10.1002/2016WR018660
- Petit C, Déverchère J (2006) Structure and evolution of the Baikal rift: a synthesis. *Geochemistry Geosystems* 7(11):1–26. doi:10.1029/2006GC001265
- Pinneker EV, Shabynin LL, Yas'ko VG, Pisarskiy BI, Pleshevenkova VA, Alekseyev VR, Leshchikov FN, Trzhtsinskiy YuB, Alekseyeva LP, Sokolov BL, Papshev MV, Lysak SV (1984) Geology and seismicity of the BAM zone. *Hydrogeology*. In: SV Krylov, KS Turitsyn. Novosibirsk, Russia
- Plusnina AM (2008) The groundwater. In: Tulohonov AK (ed) *The Baikal Lake: nature and people: encyclopedic reference book*, Ulan-Ude, Russia.
- Pola M, Fabbri P, Piccinini L, Zampieri D (2015) Conceptual and numerical models of a tectonically-controlled geothermal system: a case study of the Euganean Geothermal System, Northern Italy, Central European Geology 58(1–2):129–151. doi: 10.1556/24.58.2015.1-2-9
- Pollitz F, Vergnolle M, Calais E (2003) Fault interaction and stress triggering of twentieth century earthquakes in Mongolia. *Journal of Geophysical Research: Solid Earth* 108 (B10):2503. doi:10.1029/2002JB002375
- Pospeev AV (2012) The velocity structure of the upper mantle and regional deep thermodynamics of the Baikal rift zone. *Geodynamics & Tectonophysics* 3(4):377-383. doi:10.5800/GT-2012-3-4-0080
- Psakhier SG, Ruzhich VV, Shilko EV, Astafurov SV, Smekalin OP (2004) A study of the water saturation and vibrations effect on the displacement regime in fault zones. *Physical mesomechanics* 1:23–30.
- Shabynin LL, Pisarskiy BI, Sizykh Yu I, Orgilyanov AI (2002) Genesis and uniqueness of the Algin lakes (Transbaikal). *Geography and natural resources*. 1:116-121. (In Russ.)
- Tkachuk VG, Yasnitskaya NV, Ankudinova GA (1957) Mineral waters of the Buryat-Mongolian ASSR. Irkutsk, Russia.
- Radziminovich NA, Gileva NA, Melnikova VI, Ochkovskaya MG (2013) Seismicity of the Baikal rift system from regional network observations. *Journal of Asian Earth Sciences* 62:146–161. doi:10.1016/j.jseas.2012.10.029
- Rautian TG, Khalaturin VI, Fujita K, Mackey KG, Kendall AD (2007) Origins and methodology of the Russian energy K-class system and its relationship to magnitude scales. *Seismological Research Letters* 78(6):579-590. doi:10.1785/gssrl.78.6.579
- Reasenbergh PA, Simpson RW (1992) Response of regional seismicity to the static stress change produced by the Loma Prieta earthquake. *Science* 255(5052):1687-1690. doi:10.1126/science.255.5052.1687
- Rogers G, Dragert H (2003) Episodic tremor and slip on the Cascadia subduction zone: the chatter of silent slip. *Science* 300 (5627):1942-1943. doi:10.1126/science.1084783
- Rydelek PA, Sacks IS (2001) Migration of large earthquakes along the San Jacinto fault; stress diffusion from the 1857 Fort Tejon earthquake. *Geophys. Res. Lett.* 28 (16), 3079–3082. doi:10.1029/2001GL013005
- Saar MO, Manga M (2003) Seismicity induced by seasonal groundwater recharge at Mt. Hood, Oregon". *Earth and Planetary Science Letters* 214(3–4):605–618. doi:10.1016/S0012-821X(03)00418-7
- Shelly DR (2010) Migrating tremors illuminate complex deformation beneath the seismogenic San Andreas fault. *Nature* 436 (7281):648–652. doi:10.1038/nature08755
- Shitov AV, Kats VE, Dutova EM, Molokov VYu, Pokrovskiy VD (2016) Changes of chemical groundwater composition in the Republic of Altai due to the earthquakes. *Bulletin of the Tomsk Polytechnic University. Geo Assets Engineering* 327(1):19–29.

- Solonenko NV, Solonenko AV (1987) Aftershock sequences and swarms of earthquakes in the Baikal rift zone. Novosibirsk, Russia.
- Seminsky KZ, Tugarina MA (2011) Results of comprehensive studies of the underground hydrosphere within the western shoulder of the Baikal rift (as exemplified by the Bayandai - Krestovsky cape site). *Geodynamics & Tectonophysics* 2(2):126-144. doi:10.5800/GT-2011-2-2-0037
- Stacy S, Gerstenberger M, Williams C, Rhoades D, Christophersen A (2014) A new hybrid Coulomb/statistical model for forecasting aftershock rates. *Geophysical Journal International* 196(2):918-923. doi:10.1093/gji/ggt404
- Sherman SI (2005) Tectonophysical analysis of the seismic process in zones of lithosphere active faults and the problem of medium-term earthquake prediction. *Geophysical Journal*. 27(1):20-38
- Sherman SI (2013) Deformation waves as a trigger mechanism of seismic activity in seismic zones of the continental lithosphere. *Geodynamics & Tectonophysics* 4(2):83-117. doi:10.5800/GT-2013-4-2-0093
- Tung S, Masterlark T (2018) Delayed poroelastic triggering of the 2016 October Visso earthquake by the August Amatrice earthquake, Italy. *Geophysical Research Letters*. doi:10.1002/2017GL076453
- Tung S, Masterlark T, Dovovan T (2018) Transient poroelastic stress coupling between the 2015 M7.8 Gorkha, Nepal earthquake and its M7.3 aftershock. *Tectonophysics* 733:119-131. doi:10.1016/j.tecto.2018.02.003 2018
- Vinnik LP, Oreshin SI, Tsydypova LR, Mordvinova VV, Kobelev MM, Khritova MA, Tubanov TA (2017) Crust and mantle of the Baikal rift zone from p- and s-wave receiver functions. *Geodynamics & Tectonophysics* 8(4):695-709. doi:10.5800/GT-2017-8-4-0313
- Wang HF (2000) *Theory of Linear Poroelasticity: With Applications to Geomechanics and Hydrogeology*. Princeton University Press.
- Yoshioka R, Okuda S, Kitano Y (1970) Calcium chloride type water discharged from the Matsushiro area in connection with swarm earthquakes. *Geochemical Journal* 4:61-74.